

# Protein folding and unfolding on a complex energy landscape

Daan Thorn Leeson\*, Feng Gai†, Hector M. Rodriguez‡, Lydia M. Gregoret‡, and R. Brian Dyer†§

\*Center for Nonlinear Studies, MS B258, and †Bioscience Division, MS J586, Los Alamos National Laboratory, Los Alamos, NM 87545; and ‡Department of Chemistry and Biochemistry, University of California, Santa Cruz, CA 95064

Communicated by Hans Frauenfelder, Los Alamos National Laboratory, Los Alamos, NM, December 28, 1999 (received for review October 20, 1999)

**Recent theories of protein folding suggest that individual proteins within a large ensemble may follow different routes in conformation space from the unfolded state toward the native state and vice versa. Herein, we introduce a new type of kinetics experiment that shows how different unfolding pathways can be selected by varying the initial reaction conditions. The relaxation kinetics of the major cold shock protein of *Escherichia coli* (CspA) in response to a laser-induced temperature jump are exponential for small temperature jumps, indicative of folding through a two-state mechanism. However, for larger jumps, the kinetics become strongly nonexponential, implying the existence of multiple unfolding pathways. We provide evidence that both unfolding across an energy barrier and diffusive downhill unfolding can occur simultaneously in the same ensemble and provide the experimental requirements for these to be observed.**

The past decade has seen important advances in both theoretical and experimental studies of protein folding. Statistical mechanical treatments in combination with minimalist models of proteins have led to the introduction of a new view of protein folding that replaces the concept of folding pathways with those of energy landscapes and folding funnels (1–4). Whereas the pathway model essentially suggests that each individual protein in a large ensemble follows the same route in conformation space toward the native state, the new view pictures folding as a parallel flow process, in which individual proteins may follow different routes. Almost simultaneously with these new trends in theory, novel experimental methods have been developed that significantly improve the time resolution of kinetics studies, generally by using a short laser pulse to trigger folding or unfolding (5–10). These methods allow us to probe the critical early events in the folding process (11). Although these new developments in theory and experiment represent milestones on the road toward a fundamental understanding of the protein-folding problem, there have been only a few cases of experiments that clearly distinguish between the old view and the new view (12–15). As a consequence, significant controversy still exists about the validity of the new view (16–18).

The novel aspect of the experiments presented herein is that the relaxation kinetics were studied as a function of the *initial* conditions (in this study, the initial temperature,  $T_i$ ) at constant final conditions rather than vice versa, as is the common procedure in folding kinetics experiments in which a change either in temperature or in denaturant concentration is used to shift the equilibrium between folded and unfolded states. Whereas both a landscape model (the new view) and a pathway model (the old view) of folding can account for a dependence of the folding kinetics on the final conditions, that is, through a change of the free energy barrier, only a model that allows for multiple pathways between the folded and unfolded states can explain a dependence on the initial conditions, as will be demonstrated below.

In this report, we explore the complexity of the folding energy landscape of CspA, a predominantly  $\beta$ -sheet protein. The structure of CspA has been solved by both x-ray crystallography and nuclear magnetic resonance spectroscopy (19, 20). It is con-

structed of five  $\beta$ -strands arranged in an antiparallel barrel. An unusual structural feature of CspA is a large, solvent-exposed cluster of aromatic amino acids (21). Another distinct feature is the “cap” formed by a long loop structure that connects each half of the barrel. Cold shock proteins are among the fastest folding proteins discovered thus far. Previous folding studies of CspA and a closely related protein, *Bacillus subtilis* CspB, show very rapid folding without detectable intermediates (22–24).

Herein, we use a laser-induced temperature jump (T jump) to study the unfolding kinetics of CspA. A nanosecond IR laser pulse is absorbed by the aqueous solvent, instantaneously (with respect to the time scales of folding and unfolding) heating the sample by as much as 20°C. The T jump induces a shift in the equilibrium between the folded state and the unfolded state, and the relaxation toward the new equilibrium is monitored spectroscopically. By unfolding, we mean that the equilibrium is shifted toward a more unfolded ensemble. However, depending on the final conditions, the relaxation dynamics contain contributions from both folding and unfolding processes on a microscopic level (25). We also emphasize that, because folding and unfolding take place on the same energy surface, either folding or unfolding studies are equally well suited to characterize the folding landscape.

The relaxation dynamics are studied by probing the changes in the amide I IR absorbance of the protein backbone. The amide I IR absorbance, mainly originating from the amide C=O stretch vibration, is an established indicator of secondary and tertiary structure because of its sensitivity to hydrogen bonding, dipole–dipole interactions, and geometry of the peptide backbone (26, 27). This broad (1,610–1,680  $\text{cm}^{-1}$ ), multicomponent band contains contributions from the entire polypeptide backbone ( $\beta$ -sheet, turns, random structure). Measurements were performed at 1,623  $\text{cm}^{-1}$ , at which the absorbance originates from both loop structure and from  $\beta$ -sheet structure, and at 1,632  $\text{cm}^{-1}$ , at which the absorbance is dominated by  $\beta$ -sheet.

## Materials and Methods

The steady-state and time-resolved IR spectroscopies have been described in detail elsewhere (10). Briefly, IR spectra were obtained with a Bio-Rad model FTS-40 Fourier-transform IR spectrometer. In the time-resolved measurements, the probe is a continuous wave lead salt IR diode laser that is tunable from 1,610 to 1,700  $\text{cm}^{-1}$ . The T jump pulse is generated by Raman shifting the output of a Q switched Nd:YAG laser (Spectra-Physics), operating at 10 Hz, in  $\text{H}_2$ . Digitization of the HgCdTe IR detector (Kolmar Technologies, Conyers, GA) signal was performed by a Tektronix 7612D digitizer. Each experiment has

Abbreviations: T jump, temperature jump;  $T_i$ , initial temperature;  $T_f$ , final temperature;  $\Delta T$ , magnitude of T jump.

§To whom reprint requests should be addressed. E-mail: bdyer@lanl.gov.

The publication costs of this article were defrayed in part by page charge payment. This article must therefore be hereby marked “advertisement” in accordance with 18 U.S.C. §1734 solely to indicate this fact.

Article published online before print: *Proc. Natl. Acad. Sci. USA*, 10.1073/pnas.0405803997.  
Article and publication date are at [www.pnas.org/cgi/doi/10.1073/pnas.0405803997](http://www.pnas.org/cgi/doi/10.1073/pnas.0405803997)

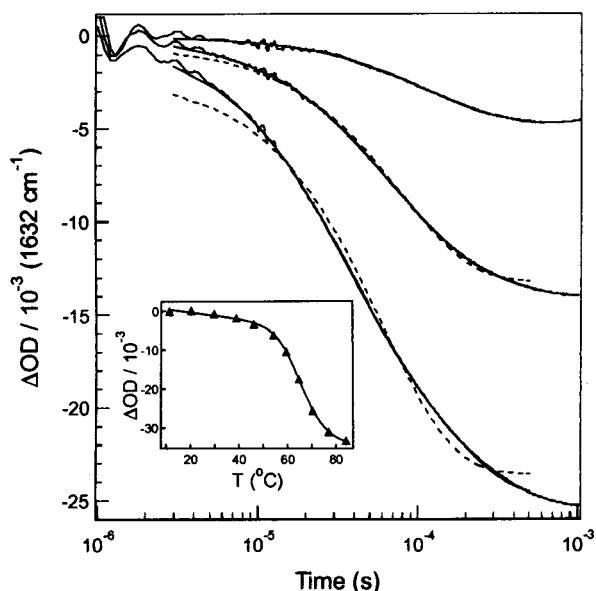


**Fig. 1.** Kinetics traces, i.e., the IR absorbance as a function of time, for T jumps from 60, 64, and 68°C (from bottom to top), all to a  $T_f$  of 80°C, recorded at 1,632  $\text{cm}^{-1}$ . The solid lines through the data are fits to a double exponential for  $T_i = 60^\circ\text{C}$  and  $T_i = 64^\circ\text{C}$  and to a single exponential for  $T_i = 68^\circ\text{C}$ . The dashed lines through the data for  $T_i = 60^\circ\text{C}$  and  $T_i = 64^\circ\text{C}$  are fits to a single exponential. The data for all  $T_i$  were also fitted to a stretched exponential function (fits not shown). All fit parameters are shown in Table 1. (Inset) Melting curve, i.e., the IR absorbance as a function of temperature, recorded at 1,632  $\text{cm}^{-1}$ . The absorbance is shown relative to its value at the lowest temperature. The solid line through the data is a fit to a two-state model plus a component linear with temperature. The fit yields a melting temperature of  $65 \pm 1^\circ\text{C}$ .

a dynamic range from  $\approx 20$  ns (limited by the detector rise time and laser pulse width) to  $\approx 1$  ms (when the solution starts to cool). The sample preparation has been described in great detail elsewhere (24).

The presence of protein aggregates at any temperature studied was excluded, based on the following arguments. (i) The IR signature of aggregates is well documented, namely, two sharp bands at 1,618 and 1,685  $\text{cm}^{-1}$ . On the basis of this fact, aggregation was observed only after prolonged (several days) exposure to high temperatures. (ii) The amide I spectrum of the protein was not affected by a temperature cycle from room temperature to 90°C and back. (iii) Aggregates act as nucleation sites for the formation of T jump-induced solvent cavities, which can be easily detected as a decreased absorption of the sample on the microsecond time scale because of scattering of the probe light. All the data presented here did not suffer from any cavitation artifact. (iv) Because aggregation generally occurs on very long time scales compared with the T jump duration, reversible aggregate formation is unlikely to occur on the time scale of our experiment.

## Results and Discussion

Fig. 1 shows kinetics traces for three T jumps, with the same final temperature,  $T_f$ , of 80°C, but with a different  $T_i$ , recorded at 1,632  $\text{cm}^{-1}$ . Fig. 1 Inset shows a steady-state melting curve recorded at the same frequency. The relaxation kinetics for the smallest T jump of 12°C are reasonably well fitted by a single exponential, indicative of a simple two-state mechanism. However, for larger T jumps, the kinetics are clearly nonexponential, and the overall decay becomes faster with decreasing values of  $T_i$ . Furthermore, with decreasing  $T_i$ , the kinetics become increas-

**Table 1.** Fit parameters for exponential, biexponential, and stretched exponential fits of data for  $T_f = 80^\circ\text{C}$  and  $T_f = 71^\circ\text{C}$

T jump, °C	$\exp(-t/\tau)$	$A_1 \exp(-t/\tau_1) + A_2 \exp(-t/\tau_2)$	$\exp[-(t/\tau)^\beta]$
60–80	$\tau = 62 \mu\text{s}$ $\chi^2 = 3.8 \times 10^{-4}$	$\tau_1 = 28 \mu\text{s}, \tau_2 = 136 \mu\text{s}$ $A_1/(A_1 + A_2) = 0.53$ $\chi^2 = 4.6 \times 10^{-6}$	$\tau = 51 \mu\text{s}$ $\beta = 0.65$ $\chi^2 = 1.9 \times 10^{-5}$
64–80	$\tau = 80 \mu\text{s}$ $\chi^2 = 3.4 \times 10^{-5}$	$\tau_1 = 46 \mu\text{s}, \tau_2 = 147 \mu\text{s}$ $A_1/(A_1 + A_2) = 0.51$ $\chi^2 = 2.6 \times 10^{-6}$	$\tau = 77 \mu\text{s}$ $\beta = 0.83$ $\chi^2 = 4.3 \times 10^{-6}$
68–80	$\tau = 116 \mu\text{s}$ $\chi^2 = 4.1 \times 10^{-6}$		$\tau = 117 \mu\text{s}$ $\beta = 0.96$ $\chi^2 = 3.9 \times 10^{-6}$
50–71	$\tau = 212 \mu\text{s}$ $\chi^2 = 1.2 \times 10^{-4}$	$\tau_1 = 99 \mu\text{s}, \tau_2 = 368 \mu\text{s}$ $A_1/(A_1 + A_2) = 0.29$ $\chi^2 = 3.1 \times 10^{-6}$	$\tau = 236 \mu\text{s}$ $\beta = 0.87$ $\chi^2 = 1.8 \times 10^{-5}$
54–71	$\tau = 267 \mu\text{s}$ $\chi^2 = 4.5 \times 10^{-5}$	$\tau_1 = 101 \mu\text{s}, \tau_2 = 397 \mu\text{s}$ $A_1/(A_1 + A_2) = 0.18$ $\chi^2 = 1.5 \times 10^{-6}$	$\tau = 309 \mu\text{s}$ $\beta = 0.89$ $\chi^2 = 3.5 \times 10^{-6}$
60–71	$\tau = 417 \mu\text{s}$ $\chi^2 = 1.0 \times 10^{-5}$		$\tau = 490 \mu\text{s}$ $\beta = 0.93$ $\chi^2 = 1.9 \times 10^{-6}$
65–71	$\tau = 437 \mu\text{s}$ $\chi^2 = 9.0 \times 10^{-6}$		$\tau = 662 \mu\text{s}$ $\beta = 0.87$ $\chi^2 = 5.8 \times 10^{-7}$

ingly nonexponential. Finally, nonexponential kinetics are observed only above a certain magnitude of the T jump,  $\Delta T$ , of approximately 12°C. For smaller values of  $\Delta T$ , exponential kinetics are observed, and there seems to be no dependence on  $T_i$ . Most decays can be equally well fitted by a biexponential or a stretched exponential decay function. However, for the most strongly nonexponential decays, i.e., for the largest T jumps, biexponential fits give significantly better results. Table 1 shows the fit parameters for exponential, biexponential, and stretched exponential fits of the data shown in Fig. 1.

For comparison, Table 1 also shows the results of fits to kinetics traces with a  $T_f$  of 71°C, again recorded at 1,632  $\text{cm}^{-1}$ . These data should be treated with caution for two reasons. First, for a  $T_f$  of 71°C, the kinetics are substantially slower than for a  $T_f$  of 80°C. Consequently, the cooling of the sample, which starts at approximately 0.5 ms, interferes with the relaxation kinetics. Consequently, the value of a quantitative analysis of the data is questionable. Second, as opposed to a  $T_f$  of 80°C, at which the final state has the dominant fraction of the ensemble in the unfolded state (which can be deduced from the melting curve shown in Fig. 1), for a  $T_f$  of 71°C, the final state still has a significant fraction of the ensemble in the folded state. Therefore, for a  $T_f$  of 71°C, the relaxation kinetics contain both contributions from folding and unfolding processes, which make interpreting the results much more difficult than for a  $T_f$  of 80°C, at which only unfolding processes contribute to the relaxation kinetics. The data for a  $T_f$  of 71°C differ from those with a  $T_f$  of 80°C in two ways. First, even for values of  $\Delta T$  below 12°C, the kinetics are slightly nonexponential. Second, for T jumps above 12°C, the kinetics are more strongly nonexponential for a  $T_f$  of 80°C than for a  $T_f$  of 71°C. Further studies will have to show whether these differences are caused by sample cooling during the relaxation or by contributions from folding processes. However, judging from the overall decay rate as measured by a fit to a single exponential, the behavior is identical, i.e., no change in the kinetics for values of  $\Delta T$  below 12°C, above which a strong increase in the relaxation rate occurs. To avoid the aforemen-

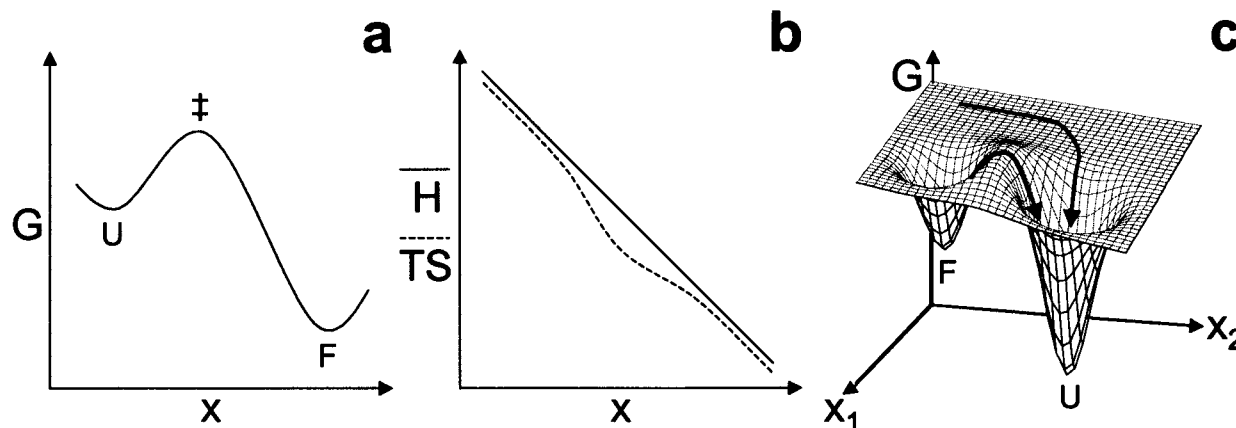


**Fig. 2.** (a) An example of a free energy diagram often used to describe protein folding and unfolding. The free energy,  $G$ , is plotted as a function of a generalized folding coordinate,  $x$ . The symbols  $U$ ,  $\ddagger$ , and  $F$  represent the unfolded ensemble, the transition state ensemble, and the folded ensemble, respectively. (b) An example of how an imperfect compensation of entropy ( $TS$ ) and enthalpy ( $H$ ) leads to a (in this case, entropic) barrier on the folding coordinate. (c) A two-dimensional free energy diagram allowing for multiple unfolding pathways.  $x_1$  and  $x_2$  represent generalized unfolding reaction coordinates.

tioned complications in interpreting the results for lower  $T_f$ , from here on, we restrict the discussion to values of  $T_f$  of 80°C and higher, at which the major contribution to the relaxation comes from unfolding processes, and we have to consider only unfolding pathways to explain the results.

Protein-folding experiments and simulations are often interpreted in terms of free energy diagrams such as the one drawn in Fig. 2a (28). These diagrams plot the free energy as a function of what is usually a loosely defined folding reaction coordinate, herein represented by the symbol  $x$ . An example of such a reaction coordinate is the fraction of native contacts. It is important to realize that each point on this coordinate does not represent a unique conformation but rather an ensemble of different conformations that have a common property, for instance, a certain number of native contacts. Because each point on the coordinate represents an ensemble of conformational states, the coordinate corresponds to an entropy [ $S = k_B \log N(x)$ , where  $k_B$  is Boltzmann's constant and  $N(x)$  is the number of states] and consequently a free energy,  $G$ . Analysis of the temperature dependence of the equilibrium coefficient and of rate coefficients between folded and unfolded states often points to the presence of a transition state ensemble, which is due to an imperfect compensation of enthalpy and entropy along the folding coordinate as shown in Fig. 2b.

The strongly nonexponential kinetics observed for large  $T$  jumps are not in agreement with a two-state description of folding along a single coordinate as shown in Fig. 2a. Given that the kinetics are exponential for a small  $T$  jump to a given  $T_f$ , a two-state model cannot explain how the kinetics become nonexponential for a larger  $T$  jump to that same  $T_f$ . Although a multistate model with either on-pathway or off-pathway intermediates could explain the nonexponential kinetics for large  $T$  jumps, it is unable to account for the dependence of the kinetics on the initial conditions—in particular, the fact that the kinetics become single exponential and do not depend on  $T_i$  for  $\Delta T < 12^\circ\text{C}$ . To explain the experimental results, we introduce the concept of a two-dimensional free energy diagram such as the one shown in Fig. 2c. The two individual coordinates,  $x_1$  and  $x_2$ , may correspond to the unfolding of different elements of secondary structure or to the unfolding of different domains of the protein. Below, we will present experimental evidence showing that, in this particular case, the two coordinates represent the unfolding of the  $\beta$ -sheets and that of the loop structure connecting each half of the  $\beta$ -barrel. As such, they may be

defined as the number of native  $\beta$ -sheet contacts and native contacts in the loop, respectively.

For a  $T_f$  of 80°C and a  $T$  jump of 20°C, a biexponential fit of the kinetics yields unfolding times of roughly 30  $\mu\text{s}$  and 0.15 ms. This large separation in unfolding times suggests that, while some protein molecules in the ensemble need to cross a free energy barrier on their way toward the unfolded state, others may proceed downhill. On a two-dimensional free energy surface, such a scenario is possible if unfolding could start from different points on the surface as indicated in Fig. 2c. The problem with this interpretation is that unfolding, by definition, starts from the folded state, which would make such a scenario highly unlikely. However, the free energy surface changes with temperature, and herein, we also suggest that the position of the folded state shifts as a function of temperature. Fig. 3 shows schematic representations of the free energy surfaces at different experimental temperatures in a way that explains all the experimental observations. Fig. 3a illustrates the case of a large  $T$  jump, i.e., one with  $\Delta T \gg 12^\circ\text{C}$ , and Fig. 3b illustrates the case of a small  $T$  jump, i.e., one with  $\Delta T < 12^\circ\text{C}$ . We emphasize that these surfaces are meant only to be considered as illustrative. They contain only the minimal amount of detail necessary to explain the experimental results. The true energy landscape is highly dimensional, and it is likely that future experiments will require additional reaction coordinates to model this complexity adequately.

If the difference between the position of the folded state at the  $T_i$  and the  $T_f$  is large enough (i.e., for a large enough  $T$  jump), then immediately after the  $T$  jump, the folded ensemble is on a metastable part of the energy surface. From this point, there are two possible scenarios, as indicated in Fig. 3a. The first is to descend into the well of the folded state on the final surface and, from there on, to attempt to cross the barrier to the unfolded state. This part of the ensemble accounts for the slow part of the relaxation kinetics. The other possibility is to proceed diffusively toward the unfolded state. This barrierless pathway is responsible for the fast part of the relaxation. Fig. 3b illustrates what happens for a  $T$  jump smaller than the “threshold value” of 12°C. If the distance between the folded states on the initial and the final surface is small enough, that is, smaller than the width of the folded state, then the folded ensemble is on a steep enough part of the energy surface to let all of the population relax back into the folded well on the final surface before crossing the barrier.

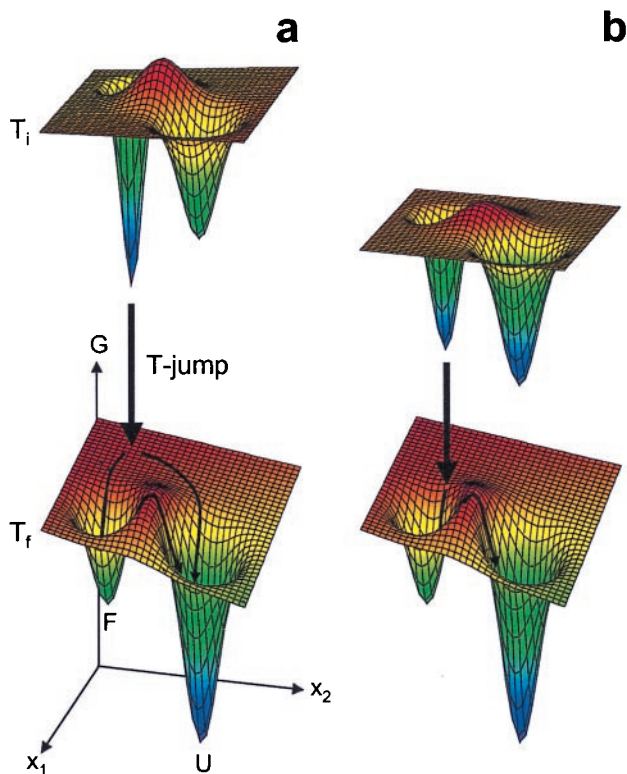


**Fig. 3.** Schematic representations of the free energy surfaces at the  $T_i$  (Upper) and  $T_f$  (Lower) of a typical T jump experiment.  $x_1$  and  $x_2$  represent generalized unfolding reaction coordinates as described in the text. The symbols  $F$  and  $U$  represent the folded and unfolded states, respectively. The downwards arrow symbolizes the T jump, and the arrows on the final surface represent the possible pathways immediately after the T jump. (a) Scenario for a large T jump. (b) Scenario for a small T jump.

There are three observations that strongly support our interpretation in terms of the free energy surfaces of Fig. 3.

(i) A major experimental clue is the previously mentioned existence of a threshold value of  $\Delta T$  to observe the fast phase in the kinetics. To direct any population along the diffusive pathway, the minimum of the folded well on the initial surface must be located outside of the folded well on the final surface. Therefore, a minimum distance between the folded states on the initial and final surfaces—and consequently a minimum value of  $\Delta T$ —is required for diffusive unfolding to occur. This concept is illustrated in Fig. 4.

(ii) For all  $T_f$ , biexponential fits of the data give a time coefficient for the slower phase that seems to be independent of  $T_i$  and that, within experimental error, is equal to the time constant of the single exponential that is found for small T jumps (see Table 1). This observation suggests that, for any T jump measured in this study, a substantial fraction of the ensemble relaxes back into the folded state on the final surface. This fraction of the ensemble will need to cross the free energy barrier toward the unfolded state and yield a contribution to the kinetics (the slow phase) that is independent of  $T_i$ .

(iii) The most compelling evidence for the shift in the folded state required to produce the multiple-pathway model presented in Fig. 3 comes from the IR kinetics and steady-state Fourier-transform IR data recorded at  $1,623\text{ cm}^{-1}$ . Fig. 5 shows a kinetics trace for a T jump from  $60^\circ\text{C}$  to  $79^\circ\text{C}$ , recorded at this frequency. Fig. 5 Inset shows the melting curve recorded at the same frequency. A large-amplitude ultrafast kinetics phase, not resolvable with the time resolution of our experimental setup, is

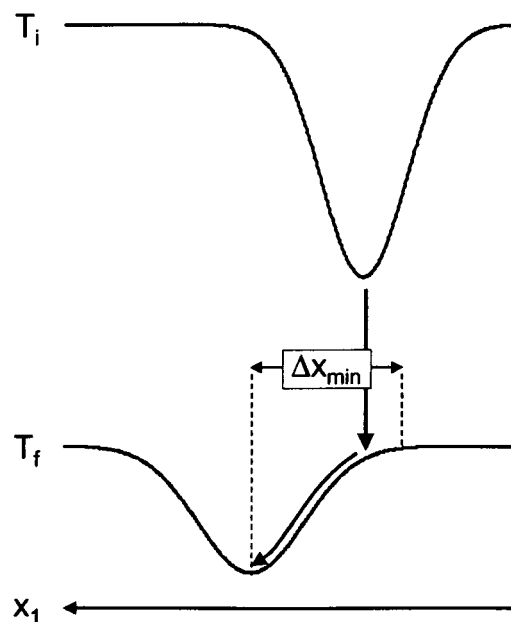


**Fig. 4.** A cross section of the free energy surface of Fig. 3 along the coordinate  $x_1$  on which the shift of the folded state occurs. The upper curve shows the folded state at the  $T_i$  of a T jump experiment, and the lower curve shows the folded state at the  $T_f$ . If the distance between the minimum of the folded state at the  $T_i$  and  $T_f$  is smaller than the threshold value,  $\Delta x_{\min}$ , then the ensemble is on a steep enough part of the surface to direct all of the population toward the folded state on the final surface. Therefore, a minimum value of the T jump exists to direct any population along the alternative diffusive pathway.

observed at this wavelength, in addition to the slower, microsecond process that dominates the kinetics measured at  $1,632\text{ cm}^{-1}$ . The ultrafast kinetics phase most likely arises from the relaxation within the folded well as indicated in Fig. 4. In fact, a small amplitude ultrafast phase is also present in the kinetics data recorded at  $1,632\text{ cm}^{-1}$ . The relative amplitude of the ultrafast phase is approximately twice as large at  $1,623\text{ cm}^{-1}$  than at  $1,632\text{ cm}^{-1}$ . Furthermore, there are clear differences in the

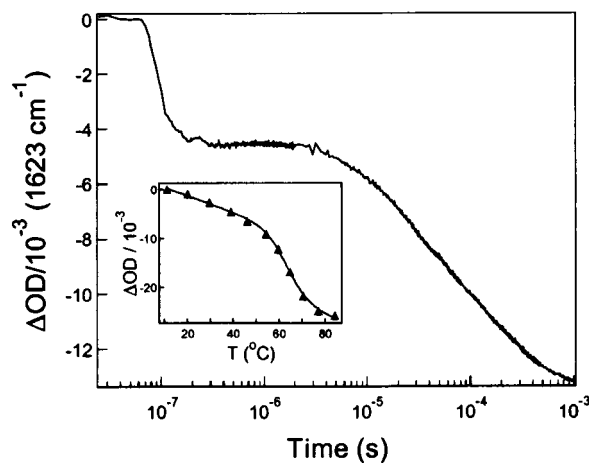


**Fig. 5.** Kinetics trace for a T jump from  $60^\circ\text{C}$  to  $79^\circ\text{C}$ , recorded at  $1,623\text{ cm}^{-1}$ . (Inset) The dependence of the absorbance at  $1,623\text{ cm}^{-1}$  on temperature. The solid line through the data is a fit to a two-state model plus a component linear with temperature.

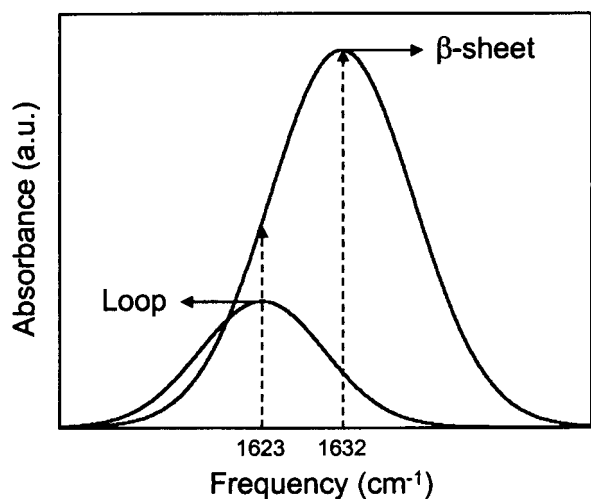


Fig. 6. A schematic representation of part of the amide I spectrum, showing how overlapping spectral components can give rise to the experimental observations.

equilibrium melting curves measured at these two wavelengths. A strong component linear in temperature is observed at 1,623  $\text{cm}^{-1}$  because of a noncooperative structural transition. The pure temperature dependence of the amide I band is small, and thus the strong linear dependence shown in Fig. 5 is due to a structural transition. A similar linear component is observed at 1,632  $\text{cm}^{-1}$  but with a substantially smaller amplitude. The relative amplitudes of the nanosecond and microsecond kinetics phases at the two wavelengths are equivalent to the relative amplitudes of the linear and cooperative components of the equilibrium melting curves at the corresponding wavelengths.

The experimental observations require the existence of at least two spectrally distinct but overlapping components of the amide I band, as illustrated in Fig. 6. The two components correspond to different structural elements of the protein that have very different kinetic and equilibrium melting behavior. The 1,623  $\text{cm}^{-1}$  band gives rise to the ultrafast kinetics phase and the linear contribution to the equilibrium transition, whereas the 1,632  $\text{cm}^{-1}$  band yields slower kinetics and a sharp, cooperative melting curve. These different spectral features must arise from different types of secondary structure of the protein. The dominant feature centered at 1,632  $\text{cm}^{-1}$  arises from  $\beta$ -sheet structure, because it is the dominant element of secondary structure of CspA. Also, 1,632  $\text{cm}^{-1}$  is a typical frequency of antiparallel  $\beta$ -sheet structure (26). The assignment of the spectral feature at 1,623  $\text{cm}^{-1}$  is less certain. The turn structures almost certainly give rise to a higher frequency amide I component at 1,668  $\text{cm}^{-1}$ , by analogy to other proteins (26). The loop structure is the only remaining major structural component of CspA. Fortunately, CspA contains a single tyrosine residue, located in the loop structure. The tyrosine side chain gives rise to a sharp band at 1,603  $\text{cm}^{-1}$  because of a ring breathing mode of the aromatic ring. The temperature dependence of this band is exactly analogous to the temperature dependence of the 1,623  $\text{cm}^{-1}$  amide I component, showing the same strong linear component. We therefore assign the 1,623  $\text{cm}^{-1}$  band to the loop structure.

The ultrafast component of the relaxation kinetics and the linear contribution to the melting curve are compelling evidence for the shift of the folded state that was required to explain the nonexponential relaxation after large T jumps. These observations are schematically illustrated in Fig. 7, which shows a

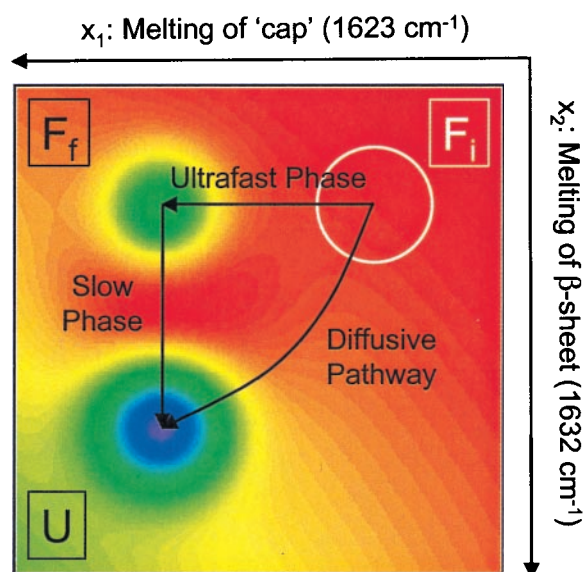


Fig. 7. A contour plot of the free energy surface of Fig. 3 at the  $T_f$ . Indicated are the various relaxation pathways from the starting point (i.e., the folded state at the  $F_f$  indicated by the white circle) toward the ending point (i.e., the unfolded state at the  $U$ ). The coordinates  $x_1$  and  $x_2$  represent the melting of the loop structure in the cap and the  $\beta$ -sheets, respectively. Because these two types of secondary structure correspond to distinct spectral components, the relative contribution of the ultrafast phase and the corresponding linear component of the melting curve depend on the frequency at which the measurement is made.

contour plot of the free energy surface at the  $T_f$ . We suggest that the folding and unfolding of the  $\beta$ -sheets and the loop structure occur independently along orthogonal coordinates  $x_1$  and  $x_2$ . The noncooperative, barrierless melting of the loop structure causes unfolding to start from a metastable part of the free energy surface for T jumps larger than the threshold value of approximately 12°C, as was illustrated in Fig. 2.

Our results and conclusions are strengthened by those of Sabelko *et al.* (15). They essentially perform a mirror image of our experiment, in the sense that they study refolding kinetics from a cold denatured state as a function of the  $T_f$  for two-domain enzyme yeast phosphoglycerate kinase and a ubiquitin mutant. First, for ubiquitin, the authors observe an ultrafast phase, indicative of relaxation into the unfolded well, analogous to the relaxation into the folded well observed in our study. Second, they observe fast downhill refolding, under conditions strongly dependent on the  $T_f$ , analogous to the downhill unfolding observed in our study.

**Summary.** Our results show how the detailed structure of the folding energy landscape can be revealed only by studying the complete range of initial and final conditions. A fascinating question is whether multiple folding pathways can be observed as well. Results obtained for  $T_f$ , at which folding and unfolding contribute in roughly equal amounts to the relaxation kinetics ( $T_f = 60$  and  $71^\circ\text{C}$ ), suggest that such an observation is indeed possible. The implication is that a fast folding pathway becomes available for large  $\Delta T$ . However, answering this question with full certainty will require an experiment under conditions in which folding dominates the relaxation kinetics.

We thank J. A. Bailey for technical assistance and K. A. Dill, A. E. Garcia, and J. Onuchic for helpful discussions. This work was supported by the National Institutes of Health.

1. Bryngelson, J. D. & Wolynes, P. G. (1987) *Proc. Natl. Acad. Sci. USA* **84**, 7524–7528.
2. Onuchic, J. N., Wolynes, P. G., Luthey-Schulten, Z. & Socci, N. D. (1995) *Proc. Natl. Acad. Sci. USA* **92**, 3626–3630.
3. Sali, A., Shakhnovich, E. & Karplus M. (1994) *Nature (London)* **369**, 248–251.
4. Dill, K. A. & Chan, H. S. (1997) *Nat. Struct. Biol.* **4**, 10–19.
5. Jones, C. M., Henry, E. R., Hu, Y., Chan, C. K., Luck, S. D., Bhuyan, A., Roder, H., Hofrichter, J. & Eaton, W. A. (1993) *Proc. Natl. Acad. Sci. USA* **90**, 11860–11864.
6. Munoz, V., Thompson, P. A., Hofrichter, J. & Eaton, W. A. (1997) *Nature (London)* **390**, 196–199.
7. Philips, C. M., Mizutani, J. & Hochstrasser, R. M. (1995) *Proc. Natl. Acad. Sci. USA* **92**, 7292–7296.
8. Ballew, R. M., Sabelko, J. & Gruebele, M. (1996) *Nat. Struct. Biol.* **3**, 923–926.
9. Pascher, T., Chesick, J. P., Winkler, J. R. & Gray, H. B. (1996) *Science* **271**, 1558–1560.
10. Williams, S., Causgrove, T. P., Gilmanshin, R., Fang, K. S., Callender, R. H., Woodruff, W. H. & Dyer, R. B. (1996) *Biochemistry* **35**, 691–697.
11. Fersht, A. R. (1997) *Curr. Opin. Struct. Biol.* **7**, 3–9.
12. Radford, S. E., Dobson, C. M. & Evans, P. A. (1992) *Nature (London)* **358**, 302–307.
13. Grantcharova, V. P., Riddle, D. S., Santiago, J. V. & Baker, D. (1998) *Nat. Struct. Biol.* **5**, 714–720.
14. Goldbeck, R. A., Thomas, Y. G., Chen, E., Esquerra, R. M. & Kliger, D. S. (1999) *Proc. Natl. Acad. Sci. USA* **96**, 2782–2787.
15. Sabelko, J., Ervin, J. & Gruebele, M. (1999) *Proc. Natl. Acad. Sci. USA* **96**, 6031–6036.
16. Laurents, D. V. & Baldwin, R. L. (1998) *Biophys. J.* **75**, 428–434.
17. Xu, Y., Mayne, L. & Englander, S. W. (1998) *Nat. Struct. Biol.* **5**, 774–778.
18. Pande, V. S., Grosberg, A. Y., Tanaka, T. & Rokhsar, D. S. (1998) *Curr. Opin. Struct. Biol.* **8**, 68–79.
19. Schindelin, H., Jiang, W., Inouye, M. & Heinemann, U. (1994) *Proc. Natl. Acad. Sci. USA* **91**, 5119–5123.
20. Newkirk, K., Feng, W., Jiang, W., Tejero, R., Emerson, S. D., Inouye, M. & Montelione, G. T. (1994) *Proc. Natl. Acad. Sci. USA* **91**, 5114–5118.
21. Hillier, B., Rodriguez, H. M. & Gregoret, L. M. (1998) *Folding Des.* **3**, 87–93.
22. Schindler, T., Herrler, M., Marahiel, M. A. & Schmid, F. X. (1995) *Nat. Struct. Biol.* **2**, 663–673.
23. Perl, D., Welker, C., Schindler, T., Schroder, K., Marahiel, M. A., Jaenicke, R. & Schmid, F. X. (1998) *Nat. Struct. Biol.* **5**, 229–235.
24. Reid, K. L., Rodriguez, H. M., Hillier, B. J. & Gregoret, L. M. (1998) *Protein Sci.* **7**, 470–479.
25. Gilmanshin, R., Williams, S., Callender, R. H., Woodruff, W. H. & Dyer, R. B. (1997) *Proc. Natl. Acad. Sci. USA* **94**, 3709–3713.
26. Susi, H. & Byler, D. M. (1986) *Methods Enzymol.* **130**, 290–311.
27. Arrondo, J. L. R., Muga, A., Castresana, J. & Goni, F. M. (1993) *Prog. Biophys. Mol. Biol.* **59**, 23–56.
28. Bryngelson, J. D. & Wolynes, P. G. (1989) *J. Phys. Chem.* **93**, 6902–6915.